

Intriguing sequence of GaFeO₃ structures and electronic states to 70 GPa

R. Arielly,¹ W. M. Xu,¹ E. Greenberg,¹ G. Kh. Rozenberg,¹ M. P. Pasternak,^{1,*} G. Garbarino,² S. Clark,³ and R. Jeanloz⁴

¹*School of Physics and Astronomy, Tel-Aviv University, 69978, Tel Aviv, Israel*

²*European Synchrotron Radiation Facility (ESRF), 6 rue Jules Horowitz, BP 220, F-38043 Grenoble Cedex, France*

³*Advanced Light Source, Lawrence Berkeley National Laboratory, Berkeley, California 94720, USA*

⁴*Department of Geology and Geophysics, University of California, Berkeley, California 94720, USA*

(Received 6 June 2011; revised manuscript received 4 August 2011; published 19 September 2011)

Structural studies of the ferrimagnetic ($T_N = 200$ K) *Mott* insulator GaFeO₃ (SG $Pc2_1n$) to 70 GPa, complemented by ⁵⁷Fe Mössbauer spectroscopy and resistance (R) measurements at compression, decompression, and recompression, reveal a fascinating sequence of structures. Starting at ~ 25 GPa a new structure, an orthorhombic perovskite (Pv) (SG $Pbnm$), is sluggishly formed followed by a volume $V(P)$ drop of 5.4%. The complete formation of the Pv occurs at 42 GPa. In the 0–33 GPa range T_N reaches 300 K and $R(P)$ decreases by one order of magnitude. At 53 GPa an isostructural transition is detected, characterized by a discontinuous drop of $V(P)$ by $\sim 3\%$. Mössbauer spectra (MS) reveal a nonmagnetic component coexisting with the magnetic one at ~ 60 GPa. Its abundance increases and above 77 GPa no sign of a magnetic hyperfine interaction is detected down to 5 K. Concurrently, one observes a continuous yet precipitous decrease in $R(P)$ taking place in the 53–68 GPa range, leading to an onset of the metallic state at $P = 68$ GPa. These electronic/magnetic features of the high pressure (HP) Pv are consistent with a *Mott* transition. With pressure decrease below 50 GPa, the insulating Pv is recovered, and at ~ 24 GPa a 1st-order structural transition takes place to a LiNbO₃-type structure with SG $R3c$. This structure remains stable down to ambient pressure and with recompression it is stable up to 50 GPa, afterwards it transforms back to the HP Pv structure. It is noteworthy that this transition occurs at the same pressure, regardless of the preceding structures: $Pbnm$ or $R3c$. The results are compared with hematite (Fe₂O₃, SG $R\bar{3}c$) and other ferric oxides. The mechanisms of the transitions are discussed.

DOI: [10.1103/PhysRevB.84.094109](https://doi.org/10.1103/PhysRevB.84.094109)

PACS number(s): 62.50.-p, 61.50.Ks, 76.80.+y, 71.30.+h

I. INTRODUCTION

Properties of the ferric oxides ($M^{3+}Fe^{3+}O_3$) at high pressure (HP) have become a subject of several recent studies.^{1,2} What has triggered the interest on the HP properties of these antiferromagnetic *Mott* insulators was the discovery³ of the electronic mechanism responsible for the unusual $\sim 10\%$ volume shrinkage observed in Fe₂O₃ (hematite) at ~ 50 GPa.⁴ In that case⁵ a pressure-induced progressive distortion of the corundum-like hematite structure was observed, preceding the transition and signifying the increasing asymmetry of the FeO₆ octahedra, which culminated in a first-order structural phase transition from a corundum to a Rh₂O₃(II)-type structure. The structural transition coincides with an insulator-metal (IM) transition and the collapse of the magnetic state (correlation breakdown). The fact that the Fe-O bonding is largely affected by the correlation breakdown implies that charge-transfer gap closure is the mechanism responsible for metallization, concurring with the collapse of the magnetic moments.

Whereas the structural transition in hematite clearly coincides with a *Mott* transition (MT) this was not the case in other ferric-oxides such as RFeO₃ ($R \equiv$ rare earth)¹ orthorhombic perovskites (Pv), where close to 40–50 GPa, a high to low spin (HS-LS) crossover takes place ($S = 5/2 \rightarrow S = 1/2$) concurrent with an isostructural phase transition and discontinuous volume reduction. Up to 170 GPa no Fe³⁺ moment collapse has been observed though an IM transition occurs at the 110–130 GPa range. It is noteworthy that in RFeO₃ orthoferites a precipitous resistance decrease was observed within the HS-LS coexistence range, suggesting that the spin crossover in the Fe sublattice approaches a gap closure and metallization transition.¹ Recent studies of BiFeO₃² have shown an onset of

a MT at ~ 50 GPa triggered, as proposed by the authors, by the HS-LS crossover, which drives the effective correlation Mott-Hubbard energy U below the threshold of the IM transition.

The purpose of this work was to further elucidate the nature of the pressure-induced electronic transitions taking place at very high pressures, e.g., spin-crossover or MT and study its role upon consequential structural transitions in ferric oxides. GaFeO₃ (GFO) with its similar Ga³⁺ and Fe³⁺ ionic radii (0.62 Å and 0.64 Å), makes it an ideal candidate for such studies, particularly with respect to FeFeO₃. The structure of GFO resulting from high temperature synthesis is orthorhombic [space group (SG) $Pc2_1n$], with two Fe and two Ga located in four different sublattices: Fe1, Fe2, and Ga2, all six-fold coordinated octahedra (O_h symmetry), and Ga1 in a four-fold coordinated tetrahedron (T_d symmetry) (see Fig. 1). Ideal stoichiometric GFO and without site disorder is an antiferromagnetic insulator with Neel temperature $T_N = 200$ K.⁶

Here we report the results of high-pressure studies to 100 GPa in diamond anvil cells (DAC) combining the methods of synchrotron powder x-ray diffraction (XRD), Mössbauer spectroscopy, and resistance studies $R(P, T)$, allowing us to follow the pressure evolutions of the GFO structure, the Fe³⁺ spin state, and the possible pressure-induced collapse of the Mott-Hubbard gap. As will be seen, a rich sequence of structural/electronic transitions takes place both at compression, decompression, and recompression.

II. EXPERIMENTAL

Samples of GaFeO₃ were prepared by solid-state reaction of stoichiometric amounts of gallic and ferric oxides. High-purity (99.999%) powders of Ga₂O₃ and 40% isotopically

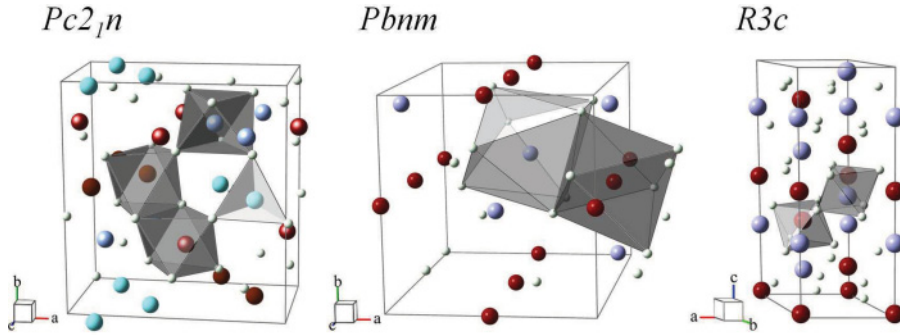


FIG. 1. (Color online) The $Pc2_1n$, $Pbnm$, and the $R3c$ crystal structures observed at various pressures in GaFeO_3 . The red/orange (shiny/mat black), blue/pale blue (shiny/mat grey), and white spheres correspond to the Fe, Ga, and O atoms at the different crystallographic sites, respectively. [Computer generated visualization based on T. C. Ozawa and S. J. Kang, *J. Appl. Cryst.* **37**, 679 (2004)].

enriched $^{57}\text{Fe}_2\text{O}_3$ were thoroughly mixed, ground, pelletized, and heated to 1300°C in an ambient atmosphere for 24 hours. After cooling for another day to room temperature, the pellet was ground, mixed, pressed, heated, and cooled again under the same conditions. Its structure and purity were verified with XRD and Mössbauer spectroscopy (see Fig. 2). As can be seen $T_N \sim 200$ K, this confirms the purity and stoichiometry of the sample.⁷ The sample was placed inside cylindrical cavities of a Re gasket following indentation to $30\text{-}\mu\text{m}$ thickness. Miniature opposing-plates and piston-cylinder DAC were used to generate pressures up to 70 and 100 GPa, respectively.^{8,9} The anvil culets ranged from 200 to $500\ \mu\text{m}$ in diameter with sample cavities from $100 \times 30\ \mu\text{m}$ to $250 \times 50\ \mu\text{m}$. Liquid Ar was loaded as a pressure medium for both Mössbauer spectroscopy and XRD studies.

Mössbauer spectra (MS) at each pressure were recorded using a 10 mCi ^{57}Co point-source in the 4–300 K temperature range. Spectra were fitted using least-squares methods from which MS parameters were deduced: specifically, the relative abundance of the components, the hyperfine field $H_{\text{hf}}(P)$, the

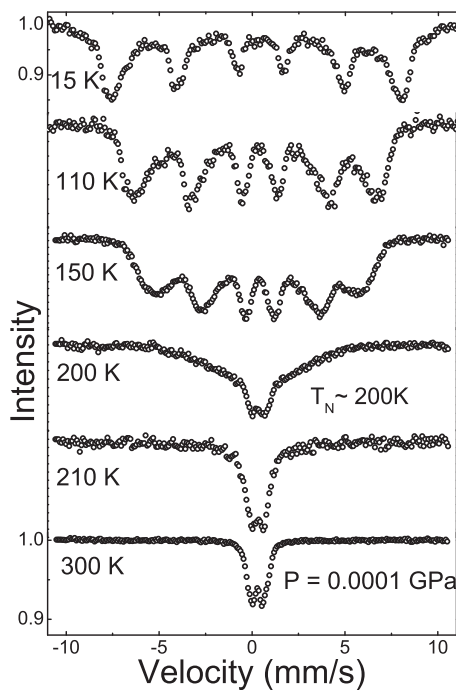


FIG. 2. MS in the 15–300 K range from which $T_N \approx 200$ K has been derived. This value is consistent with a stoichiometric composition and minimal disorder.

isomer shift $IS(P)$, the quadrupole splitting $QS(P)$, and the magnetic ordering temperature $T_N(P)$.

It should be noted that the complete decomposition of the magnetic and paramagnetic subspectra of the four crystallographic sites of Fe could not be carried out due to the finite resolution of the ^{57}Fe Mössbauer spectroscopy governed by its line width. However, taking into account the similarity in the crystallographic surroundings for more than 90% of the Iron,⁶ the spectra could be safely fitted using one component¹⁰ with a relatively broad line width.

XRD measurements were carried out at room temperature in angle-dispersive mode with wavelength of $0.3738\ \text{\AA}$ and $0.41336\ \text{\AA}$ at ESRF, Grenoble, at the ID27 beam line and at ALS, Berkeley, at beam line 12.2.2, respectively. Diffraction images were collected using image plates or CCD. The image data were integrated using the FIT2D program,^{11,12} and the resulting diffraction patterns were analyzed with the GSAS^{13,14} program.

Ruby R_1 -line fluorescence spectroscopy was used^{15–17} as a manometer for the Mössbauer spectroscopy and $R(P)$ studies; Pt¹⁸ pressure markers were used for the XRD measurements.

Four-probe DC electrical-resistance measurements as a function of pressure and temperature were carried using a stainless-steel gasket coated with Al_2O_3 into which a sample cavity of $\sim 100\text{-}\mu\text{m}$ diameter was hand-drilled. Six electrodes of $5\text{--}7\text{-}\mu\text{m}$ -thick Pt-foils were employed. At each pressure, the DAC was immersed inside a liquid N_2 -filled Dewar for measurements over the 80–300 K range. Temperature was determined using a Si-diode thermometer, and resistance values were derived from the measured I–V curves. Typical errors associated with pressure and temperature were ± 1 GPa and ± 0.5 K, respectively.

Experiments were carried out in the following pressure cycles: 1—XRD, ^{57}Fe Mössbauer spectroscopy, and $R(P, T)$ measurements were carried during compression to 98 GPa; 2—XRD and ^{57}Fe Mössbauer spectroscopy at decompression to ambient pressure; and 3—XRD at recompression to 53 GPa.

III. RESULTS

Typical examples of full-profile fitted XRD spectra of the three structures emerged from this experiment, at pressure values in which there is no phase coexistence, are shown in Fig. 3: (i) the orthorhombic $Pc2_1n$ ($Z = 8$) phase which persists from ambient pressure to ~ 40 GPa, (ii) the orthorhombic Pv (SG $Pbnm$ $Z = 4$) present above 25 GPa both at compression and decompression, and (iii) the LiNbO_3 -type phase (SG $R3c$ $Z = 6$) which emerged during decompression at 24 GPa and

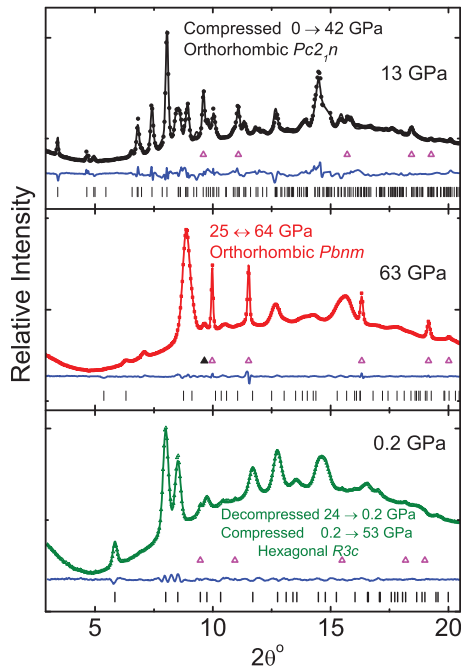


FIG. 3. (Color online) Typical examples of analyzed integrated patterns of XRD spectra collected for the three main crystallographic structures at various stages of compression/decompression at 13, 63, and 0.2 GPa at RT and the differences between the observed and calculated profiles. Marks show the calculated peak positions. The Δ symbols correspond to the Pt-pressure marker, \blacktriangle to FeO contamination (<5%).

persisted down to ambient pressure. During recompression the $R3c$ phase persists up to ~ 50 GPa after which it transforms to the orthorhombic Pv ($Pbnm$). In Fig. 4 we recap the Equation of State (EOS), namely, $V(P)$ of the three pressure paths: compression (filled symbols), decompression (open symbols), and recompression (filled symbols).

A. Compression

1. The 0 \rightarrow 50 GPa isotherm

(a) Structural properties (see Figs. 3 and 4). Up to 25 GPa the $Pc2_1n$ symmetry is dominant with gradual volume decrease from 312 \AA^3 at ambient pressure to 273 \AA^3 at 42 GPa. In this range the XRD data was successfully fitted by solely varying the three lattice parameters with atomic positions fixed to those at ambient pressure¹⁹ resulting in $\chi^2 < 0.12$, $w_{Rp} < 1.5\%$, and $R_p < 1\%$. The refined structural parameters obtained from the GSAS software are shown in Table I. The $P(V)$ data for the $Pc2_1n$ phase was fitted to the 2nd-order Birch-Murnaghan (BM2) EOS²⁰ up to 40 GPa while fixing the first derivative of the bulk modulus to $K' = 4$. The unit-cell volume as a function of pressure is shown in Fig. 4. The resulting ambient pressure unit-cell volume and bulk modulus are $V_0 = 312.2(4) \text{ \AA}^3$ and $K_0 = 230(4) \text{ GPa}$, respectively.

At ~ 25 GPa a new phase starts evolving at the expense of the $Pc2_1n$. It is identified as the orthorhombic Pv with SG $Pbnm$ (Fig. 1). This phase can also be characterized in an orthorhombic setting by the three lattice parameters a , b , and c , but with only four possible atomic positions. Following studies

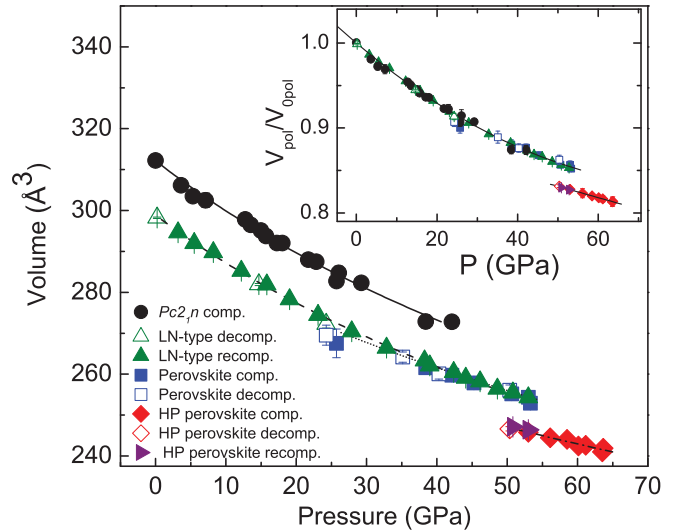


FIG. 4. (Color online) Pressure evolution of the unit cells volume of GaFeO₃. The solid, dotted, dash-dotted, and dashed lines are theoretical fits for the $Pc2_1n$, LP Pv, HP Pv, and LiNbO₃ (LN)-type phases using the BM2 EOS. The variables obtained were: $K_0 = 230(4) \text{ GPa}$, $V_0 = 312.2(4) \text{ \AA}^3$ for the $Pc2_1n$ structure; $K_0 = 296(25) \text{ GPa}$, $V_0 = 291.7(2.4) \text{ \AA}^3$ for the LP Pv structure; $K_0 = 383(48) \text{ GPa}$, $V_0 = 274.6(4.4) \text{ \AA}^3$ for the HP Pv structure, and $K_0 = 223(9) \text{ GPa}$, $V_0 = 298.7(8) \text{ \AA}^3$ for the LN-type at decompression and recompression. The volume was normalized to six unit formulas of GaFeO₃, i.e., $Z = 8$ for $Pc2_1n$ phase, $Z = 4$ for $Pbnm$ orthorhombic Pv, and $Z = 6$ for LiNbO₃-type $R3c$ phase. The inset shows the relative volume of the FeO₆ polyhedron for all phases as a function of pressure. Note the polyhedron volume drop at $V_{pol}/V_{opol} \sim 0.85$. The solid and open symbols correspond to the compression and decompression cycles, respectively.

of the rare earth orthoferrites (SG $Pbnm$) by Marezio *et al.*,²¹ the atomic positions have been extrapolated according to the cation size of Ga. The data was successfully fitted by solely varying the three lattice parameters, with atomic positions fixed to the values extrapolated for ambient pressure, resulting in χ^2 being less than 0.025, $w_{Rp} < 0.6\%$ and $R_p < 0.4\%$. The refined structural parameters are shown in Table I. The transition to the Pv phase is accompanied by a discontinuous volume change of -5.4% (Fig. 4). The dotted line is a fit using a Birch-Murnaghan EOS resulting in $K_0 = 296(25) \text{ GPa}$, $K_0' = 4$ (fixed), and $V_0 = 291.7(2.4) \text{ \AA}^3$. Unlike the orthorhombic $Pc2_1n$ phase, there is only one cationic site for Fe (six-fold coordinated) and one for Ga (eight-fold coordinated) (Fig. 2). The coordination increase in Ga from four and six to eight is a possible leading mechanism behind this phase transition and the significant discontinuous volume decrease. Above 42 GPa only the Pv structure is observed.

(b) Electronic and magnetic properties. Consistent with the volume decrease, the magnetic exchange interactions, and therefore the ordering temperature, increases with pressure (Fig. 5), starting from 200 K at ambient pressure and reaching 300 K at ~ 33 GPa. At $P > 33$ GPa $T_N(P)$ increases beyond 300 K but could not be quantified due to high temperature experimental limitations of the present MS system. Typical spectra at 15 K ($T < T_N$) is shown in Fig. 6. Up to 56 GPa there are no discernible changes in the low temperature MS in

TABLE I. The refined structural parameters of the $Pc2_1n$ and of the $Pbnm$ perovskite (compression and decompression) phases at various pressures. *Italic* represents data from the decompress cycle.

P(GPa)	$a(\text{\AA})$	$b(\text{\AA})$	$c(\text{\AA})$
<i>Pc2_{1n} phases</i>			
0.0001	8.7347(14)	9.3850(15)	5.0791(9)
3.6	8.649(11)	9.306(14)	5.072(9)
5.3	8.634(18)	9.27(2)	5.057(13)
7.1	8.640(26)	9.246(30)	5.05(2)
12.7	8.580(7)	9.210(6)	5.025(5)
13.5	8.54(1)	9.185(8)	5.041(6)
15.0	8.580(22)	9.14(3)	5.017(16)
15.7	8.554(12)	9.136(10)	5.013(7)
17.2	8.487(12)	9.137(10)	5.022(6)
18.0	8.503(12)	9.145(23)	5.008(14)
21.7	8.502(11)	9.038(10)	4.9970(45)
22.8	8.384(23)	9.10 0(24)	5.023(20)
25.7	8.417(15)	9.005(16)	4.974(20)
26.1	8.303(26)	9.034(30)	5.063(20)
29.3	8.240(18)	9.043(25)	5.052(16)
38.4	8.370(35)	8.80 0(18)	4.94(2)
42.1	8.387(24)	8.792(20)	4.933(23)
<i>LP perovskite phase</i>			
25.7	4.948(4)	5.165(20)	7.000(8)
38.4	4.948(12)	5.077(20)	6.963(9)
42.1	4.946(10)	5.068(14)	6.947(10)
45.3	4.917(10)	5.066(13)	6.922(10)
50.6	4.926(10)	5.015(11)	6.884(8)
53.3	4.893(8)	5.035(7)	6.870(9)
53.0	4.904(13)	5.025(16)	6.902(10)
50.3	4.942(17)	5.023(20)	6.897(8)
40.3	4.937(16)	5.080(17)	6.941(8)
35.1	4.971(6)	5.110(23)	6.955(7)
24.1	4.991(10)	5.142(18)	7.020(16)
<i>HP perovskite phase</i>			
53.0	4.795(10)	4.950(12)	6.925(14)
56.1	4.796(10)	4.942(20)	6.897(23)
58.5	4.788(5)	4.939(6)	6.886(8)
61.2	4.782(10)	4.935(11)	6.882(12)
60.1	4.784(4)	4.922(13)	6.886(10)
63.6	4.7754(30)	4.924(20)	6.870(17)
63.5	4.775(3)	4.92(2)	6.874(20)
50.3	4.793(6)	4.968(4)	6.937(7)

which the single component displays a magnetic splitting with $H_{\text{hf}} = 48(3)$ T.

The relative volume ($\Delta V/V_0$) dependence of the IS is shown in Fig. 7.²² The slope $d(\text{IS})/d\ln(V)$, an atomic-scale property, remains rather constant and monotonic within the $Pc2_1n$ region and up to $\Delta V/V_0 = 0.22$ (~ 60 GPa) This is in spite of the transition to the Pv structure starting around 0.11 (~ 25 GPa) with its discontinuous volume decrease of $\sim 5\%$. The reason being that the IS is directly related to the s -electron density $\rho_s(0)$ at the Fe nucleus.²³ Thus, upon pressure increase the density at the Fe vicinity increases, as expected, but it is not affected by the volume decrease taking place due to the discontinuous increase in the Ga coordination number.

Within the 0–31 GPa range ($Pc2_1n$ region), $R(\Delta V/V)$ decreases by one order of magnitude (see Fig. 8). At higher

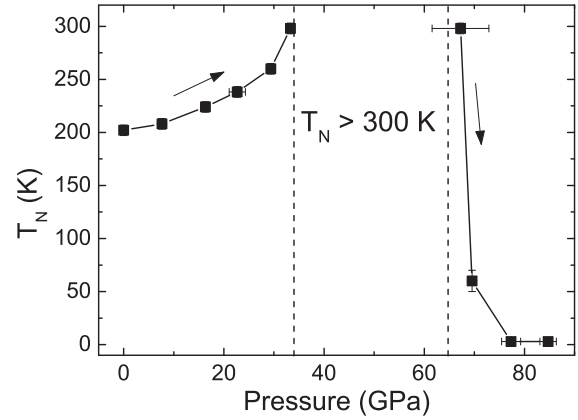


FIG. 5. Pressure dependence of the magnetic ordering temperature T_N . It reaches 300 K at ~ 33 GPa and in the 33–67 GPa pressure range $T_N > 300$ K. At 67 GPa it decreases to RT after which T_N precipitously reaches ~ 5 K at 77 GPa.

pressures, within the pure $Pbnm$ region (42–53 GPa range and up to $\Delta V/V_0 = 0.2$), $R(P)$ variation is more gradual. However, as shown in the lower inset, in this pressure range there is a continuous flattening of the $R(T)$ curves with pressure increase due to a decrease in the activation energy, as expected from band broadening.²⁴

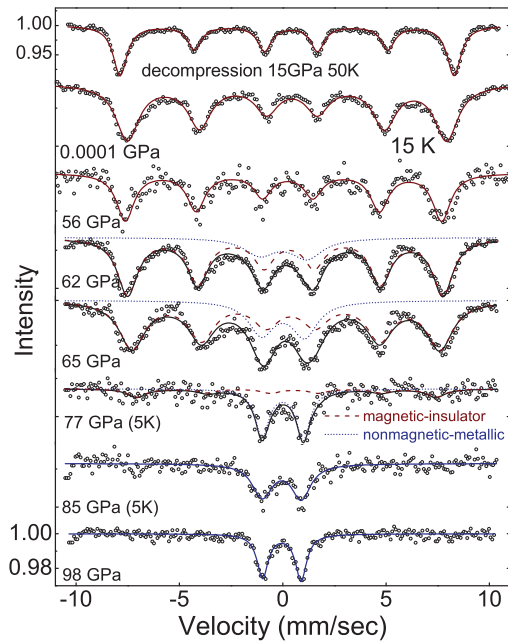


FIG. 6. (Color online) MS recorded at 15 K for various pressures. The H_{hf} is typical of the Fe^{3+} oxides and reflects the magnetization at saturation ($T \ll T_N$) as a function of pressure. Up to 56 GPa this is the only spectral component. At 62 GPa a nonmagnetic quadrupole-split component (dotted line) appears with relative abundance increasing with pressure. There is no apparent spectral change up to 98 GPa. The absence of magnetic components down to the lowest temperature of 5 K (85 GPa spectrum) strongly supports the onset of the MT characterized by the magnetic collapse due to the d - d correlation breakdown. The decompression spectrum does not show any sign of *sites distributions*.

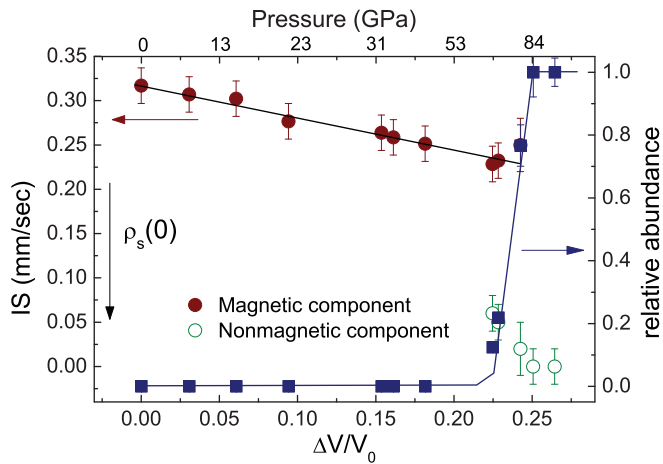


FIG. 7. (Color online) The pressure dependence of the IS (red-filled circle, white circle) and the relative abundance (blue-filled square) of the nucleated metallic-nonmagnetic GaFeO₃. Their functional dependence upon $\Delta V/V_0$ where $\Delta V = |V - V_0|$ reflects the proper variation of the molar volume shrinkage considering the fact that along the P -path various structures emerge with diverse bulk modulus values. As can be seen the IS decreases with pressure, namely the s -density at the nucleus ρ_s increases linearly with the fractional decrease of the molar volume. At 0.225 ($P \sim 62$ GPa) an abrupt drop in the IS is observed, corresponding to an abrupt increase in the $\rho_s(\Delta V/V_0)$, signaling the sharp decrease of the $\langle \text{Fe-O} \rangle$ distances. At the same $\Delta V/V_0$ value one observes a drastic increase in the metallic nonmagnetic component reaching 100% at ~ 80 GPa.

2. The 50 \rightarrow 68 GPa isotherm

(a) Structural evolution. At ~ 53 GPa we witness (Fig. 4) a discontinuous reduction in volume $\Delta V/V_0 \sim 3\%$. This structural transition carries no change in SG, namely, an isostructural transition. The data was successfully fitted by solely varying the three lattice parameters resulting in $\chi^2 < 0.055$, $w_{\text{Rp}} < 0.8\%$, and $\text{Rp} < 0.6\%$. The refined structural parameters are shown in Table I. The HP Pv phase coexists with the lower pressure (LP) Pv phase in the 53–54 GPa range. The dash-dotted line is a fit using a Birch-Murnaghan EOS with variables $K_0 = 383(48)$ GPa, $K_0' = 4$ (fixed), and $V_0 = 275(4) \text{ \AA}^3$.

(b) Electronic and magnetic properties. The MS(P) clearly shows a sluggish onset of a nonmagnetic, quadrupole-split component, at $P > 56$ GPa coexisting with the magnetic component (Fig. 6). Its abundance increases with P , and beyond 65 GPa this component becomes dominant. To ensure the absence of magnetism at lower temperatures characterized by the magnetic hyperfine interaction, spectra at $P > 65$ GPa were also recorded at 5 K.²⁵ As can be seen, the spectrum at 77 GPa and 5 K, in spite of the bad statistic, still shows remnants of a magnetic interaction component, characterized by H_{hf} of ~ 45 T. However, the spectrum at 85 GPa shows no indications of magnetic interactions. The significant changes are also seen in $T_N(P)$ (Fig. 5). Above 33 GPa $T_N(P)$ crosses 300 K and near 67 GPa, while descending, it crosses 300 K again, reaching $T_N \sim 5$ K at 77 GPa. The IS($\Delta V/V_0$) curve shows a discontinuous sharp decrease in the 0.225–0.24 range (62–77 GPa) (Fig. 7). The relative abundance of the nonmagnetic-metallic phase associated with the HP-Pv structure and derived from

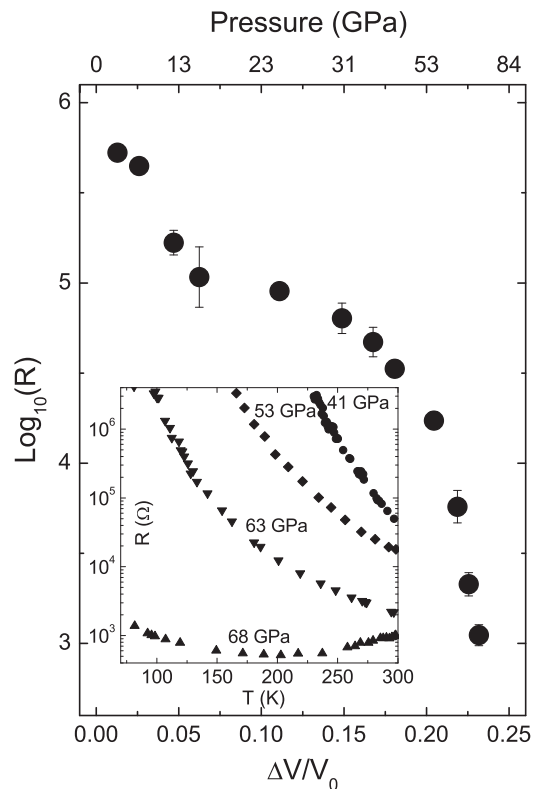


FIG. 8. The variation of $R(P)$ with $\Delta V/V_0$ at RT. A sharp decrease in R is observed in the 0–0.08 $\Delta V/V_0$ range (0–20 GPa) taking place at the $Pc2_1n$ phase. Following the onset of the Pv phase the change in $R(P)$ is more gradual till $\Delta V/V_0 \sim 0.20$, where the electrons delocalization is triggered by d - d or p - d gap closure, reaching a metallic state at $P \sim 68$ GPa (see lower inset). The $R(\Delta V/V_0)$ behavior in this range is very similar to that of $\rho_s(\Delta V/V_0)$ in the same pressure range (see Fig. 7) in accordance with the MT concept.

the MS²⁶ increase sharply around $\Delta V/V_0 = 0.22$ reaching 1 at ~ 0.24 (~ 80 GPa) (see Fig. 7). Concurrently, one observes (Fig. 8) a continuous yet precipitous decrease in $R(\Delta V/V_0, 300 \text{ K})$ taking place in the 0.20–0.23 range (53–68 GPa), leading to the onset of the metallic state at $P \sim 68$ GPa evident by the partially positive dR/dT (lower inset).

B. Decompression

1. The 68 \rightarrow 24 GPa isotherm (see Fig. 4)

With decompression the HP-Pv structure dominates down to 50 GPa. At ~ 50 GPa it undergoes a discontinuous increase in V , with no hysteresis, eventually recovering the original LP-Pv structure and volume (Fig. 4, open symbols) characterized by its larger Fe³⁺-O bond lengths reflecting the recovery of the correlated state.

2. The 24 \rightarrow 0 GPa isotherm (Fig. 4)

At 24 GPa a dramatic structural first-order transition takes place. Diffraction patterns of the new phase can be fitted well with three different structures: corundum-type trigonal (SG $R\bar{3}c$), ilmenite FeTiO₃-type (SG $R\bar{3}$) or LiNbO₃ (LN)-type (SG $R\bar{3}c$). Taking into account that the derived c/a ratio of 2.699 is more typical for a LN structure than for ilmenite,

as well as the better quality of the fit results assuming a LN-phase, we discarded the ilmenite-type option. Although $R3c$ and $R\bar{3}c$ structures show very similar quality of the fit, typically $\chi^2 \sim 0.017$, $W_{RP} < 0.46\%$, and $R_p < 0.36\%$, one must take into account that the corundum-type structure does not differentiate between Ga and Fe sites, which will result in random positions of the Fe-magnetic moments leading to a disorder in the magnetic sublattices. In that case the MS would have shown features typical of *sites distributions*, e.g., broad and asymmetric absorption lines, which is not the case (Fig. 6). These arguments definitely favor the assignment of the new structure as the hexagonal LiNbO_3 -type phase (Fig. 1).²⁷ This phase can be characterized in a hexagonal setting by two lattice parameters, a and c , and three possible atomic positions. The latter values were taken from the work of Boysen *et al.*²⁸ and further refined for the spectrum at 0.2 GPa. Using the obtained atomic positions the data was successfully fitted by solely varying the two lattice constants. The refined structural parameters are shown in Table II. The transition to the LN structure is accompanied by a small discontinuous increase in V (Fig. 4). This structure persists down to ambient pressure; the original $Pc2_1n$ phase is not recovered.

C. Recompression

1. The $0 \rightarrow 53$ GPa isotherm (see Fig. 4 and Table II)

With recompression to ~ 50 GPa the $R3c$ phase is fully preserved. The dashed line is a fit to all of the $R3c$ points using a Birch-Murnaghan EOS with variables $K_0 = 223(9)$ GPa, $K_0' = 4$ (fixed), and $V_0 = 298.7(8) \text{ \AA}^3$. The gradual shrinkage in volume, especially around 24 GPa, is not energetically sufficient to recover the $Pbnm$ Pv state. The phase is stable up to ~ 50 GPa, yet again at 50 GPa, due to the Fe^{3+} -O bond length shrinkage, the LiNbO_3 -type structure becomes unstable and is replaced by the sturdier HP-Pv structure.

IV. DISCUSSION

By examining the $\text{MS}(P, T \ll T_N)$, $\text{IS}(\Delta V/V_0)$, and $R(\Delta V/V_0, T)$ data, as shown in Figs. 6–8, one comes to the conclusion that the breakdown of the magnetic moment along with evidence of a metallic behavior coincides with the MT leading to the breakdown of the strong d - d correlation and therefore to the IM transition. At the compression isotherm one notices the striking features of $R(\Delta V/V_0)$, $\rho_s(\Delta V/V_0)$, and the nonmagnetic relative abundance $(\Delta V/V_0)$ (Figs. 7 and 8), a convincing experimental evidence of this unusual electronic transition, e.g., the MT in Fe^{3+} .

Close to the critical pressure, when the Hubbard gap is small enough, electrons can be excited into the conduction band. In that case disordering of the moments due to their coupling with the excited electrons should be observed.²⁹ Such or similar changes of the electronic properties of the insulating magnetic phase near to the MT will result in the weakening of the super-exchange interactions and consequently in the drop in T_N (Fig. 5). Ultimately GaFeO_3 becomes nonmagnetic and metallic at $P > 77$ GPa. Preceding this state a region of paramagnetic/nonmagnetic coexistence should exist, in which insulating clusters of Fe^{3+} moments ($S = 5/2$) and conducting

TABLE II. the refined structural parameters of the LN-type and HP perovskite(decompression and recompression) phases at various pressures. Italic represents data from the decompression cycle.

$P^*(\text{GPa})$	$a(\text{\AA})$	$b(\text{\AA})$	$c(\text{\AA})$
LN phase			
24.3	4.920(8)	4.920(8)	13.00(4)
14.7	4.968(2)	4.968(2)	13.188(10)
0.2	5.036(2)	5.036(2)	13.585(7)
3.2	5.0235(14)	5.0235(14)	13.480(5)
5.5	5.0094(12)	5.0094(12)	13.436(5)
8.2	4.9977(13)	4.9977(13)	13.397(5)
12.2	4.9737(15)	4.9737(15)	13.314(6)
15.8	4.9570(14)	4.9570(14)	13.245(5)
19.1	4.9378(14)	4.9378(14)	13.179(5)
23.1	4.9172(15)	4.9172(15)	13.105(6)
27.9	4.8967(17)	4.8967(17)	13.023(6)
32.9	4.8765(18)	4.8765(18)	12.936(6)
38.3	4.8607(17)	4.8607(17)	12.867(6)
39.0	4.8550(17)	4.8550(17)	12.839(6)
42.4	4.849(2)	4.849(2)	12.790(7)
44.1	4.844(2)	4.844(2)	12.751(7)
46.2	4.8423(20)	4.8423(20)	12.714(8)
48.6	4.8390(27)	4.8390(27)	12.644(9)
50.8	4.824(5)	4.824(5)	12.672(10)
52.8	4.815(7)	4.815(7)	12.665(13)
HP perovskite phase			
50.8	4.794(10)	4.954(6)	6.937(10)
52.8	4.784(8)	4.950(4)	6.937(9)

nonmagnetic clusters coexist, the latter becoming dominant at $P > 68$ GPa.

Thus, the onset of the MT may explain the observed alterations of the structural, electronic, and magnetic properties at pressures above 53 GPa. However, in spite of the sharp first-order structural transition observed at $P \sim 53$ GPa, changes in the electronic/magnetic properties measured with MS and R take place above 53 GPa and continue sluggishly up to ~ 80 GPa. A systematic reason could be the two different types of manometries: the use of a Pt marker from which the pressure is deduced from the supposedly well-known Pt-EOS and the ruby method. Another systematic reason could be the different geometries of the signal collection methods: the pressure is usually measured in the center of the sample cavity. Also, in the synchrotron XRD measurements the signal derives from a small central part of the sample, whereas in Mössbauer studies the signal is collected from a much larger; $\sim 2/3$ of the sample diameter, resulting in possible pressure gradient effects, which could be significant. In resistivity measurements the role of pressure gradients could be also substantial.³⁰ It is important to note that in the 50–53 GPa range the MS do not reveal any evidence of a preceding electronic transition, such as a spin-crossover, which could account for the observed volume decrease.

It will be interesting to compare the present results with the other $M\text{FeO}_3$ oxides in which XRD, spectroscopy, and/or resistance were concurrently applied. As mentioned earlier, the $R\text{FeO}_3$ orthoferrites are an exception in the sense that at HP they undergo spin crossover ($S = 5/2 \rightarrow S = 1/2$)

transition at the 35–50 GPa range but do not undergo a MT to at least 170 GPa.¹ In what follows we compare GaFeO₃ with hematite (FeFeO₃)³ and CaFe₂O₄.³¹ A common feature of all those ferric oxides is the discontinuous volume contraction occurring at ~50 GPa, when the relative volume of the Fe-O₆ polyhedral $V_{\text{pol}}/V_{0\text{pol}}$ reaches 0.84–0.85.

Hematite at ambient conditions crystallizes in a corundum structure ($R\bar{3}c$) with six-coordinated Fe³⁺. GaFeO₃ on the other hand, when synthesized at ambient pressure, crystallizes in an orthorhombic structure with SG $Pc2_1n$. Unlike hematite GaFeO₃ has two six-coordinated Fe-sites, one six-coordinated Ga-site, and one four-coordinated Ga-site. It is not surprising that this partially low-coordination species will not withstand the high-density regime. And indeed, a first-order structural phase transition takes place at ~25 GPa ($V/V_0 \sim 0.91$) into a sturdier orthorhombic Pv ($Pbnm$) with a single six-coordinated Fe-O and a single eight-coordinated Ga-O building block. The molar volume of the Pv is reduced by ~5%, and its bulk modulus increases by ~30%. With further pressure increase a second, albeit isostructural, phase transition takes place at ~53 GPa ($V_{\text{pol}}/V_{0\text{pol}} \sim 0.85$, see inset Fig. 4) with a discontinuous volume decrease of ~3%. This reversible transition is concomitant with the *Mott* electronic transition of Fe³⁺, the same one observed in Fe₂O₃,³ in which the high-spin is transformed to a nonmagnetic state.

Contrary to hematite, following decompression to ambient pressure, the $R3c$ structure becomes the stable one. The reason that upon decompression Pv transform to LN-type instead of the original $Pc2_1n$ is a close structural relation of the LN- and Pv-type structures.^{32,33} Both structures consist of corner-linked FeO₆ octahedra, but in the Pv-type structure the adjacent octahedral layers are less tilted relative to one another. Therefore, in contrast to the $Pc2_1n$ structure, the octahedral framework can readily transform between the two structures by rotating them as rigid units without breaking any bonds. The V_0 of the $R3c$ phase is ~5% smaller than that of the $Pc2_1n$ phase but its bulk modulus K_0 remains almost the same and is practically identical to that of hematite.^{4,34,35} At recompression the first-order structural phase transition takes place again at $P \sim 50$ GPa ($V_{\text{pol}}/V_{0\text{pol}} \sim 0.85$), exactly as in Fe₂O₃ ($P \sim 50$ GPa, $V_{\text{pol}}/V_{0\text{pol}} \sim 0.84$).^{4,5} The relative volume reduction at this point remains ~3%, whereas in Fe₂O₃ it is ~10%. However, taking into account the corroborating transformation from corundum to Rh₂O₃-II structure,³⁶ the part of the volume reduction associated with the electronic transition in Fe₂O₃ is

~6%, scaling well with the Fe/formula number: 1 in GaFeO₃ and 2 in Fe₂O₃. The corresponding shrinkage of the polyhedral volume in both systems is ~6%.

HP-XRD studies in CaFe₂O₄ (SG $Pbnm$) also reveal an abrupt volume decrease at 50 GPa ($V_{\text{pol}}/V_{0\text{pol}} \sim 0.84$). Though no $R(P, T)$ measurements were carried out, magnetic collapse is clearly observed by M. Merlini *et al.*³⁰ by x-ray emission spectroscopy and is consistent with a MT. However, in the case of CaFe₂O₄ the corresponding abrupt polyhedral volume decrease is ~12%, doubled in comparison to GFO and Fe₂O₃. Such a decrease is in good agreement with the values tabulated by Shannon³⁷ for high- and low-spin states. Additional Mössbauer spectroscopy and $R(P, T)$ are necessary in this case to clear an exact mechanism of the electronic transition.

V. CONCLUSIONS

In conclusion a series of structural, electronic, and magnetic transitions was observed in GaFeO₃ at the 0–70 GPa range. The structural instability of the partially low-coordination $Pc2_1n$ lattice results beyond 25 GPa in the more sturdier Pv $Pbnm$ structure, which undergoes at ~53 GPa the reversible isostructural transition corroborating with the *Mott* electronic transition to the uncorrelated HP Pv. Following decompression, the structurally related $R3c$ structure becomes the stable one below 24 GPa, but at recompression it is replaced by the uncorrelated HP Pv at ~50 GPa. Comparison of the present results with the FeFeO₃ and CaFe₂O₄ data allows concluding that in all these ferric oxides the electronic transition to the uncorrelated state occurs at the same pressure, regardless of the preceding structures: $Pbnm$, $R3c$, or $R\bar{3}c$, when the relative volume of the Fe-O₆ polyhedral $V_{\text{pol}}/V_{0\text{pol}}$ reaches 0.84–0.85.

ACKNOWLEDGMENTS

This research was supported in part by Israeli Science Foundation Grant #789/10 and the US National Science Foundation and Department of Energy. We acknowledge the European Synchrotron Radiation Facility for provision of synchrotron radiation facilities beam line ID27. The Advanced Light Source is supported by the Director, Office of Science, Office of Basic Energy Sciences, of the US Department of Energy under Contract No. DE-AC02-05CH11231. The DAC's were provided in kind by D'Anvils Ltd. (www.danvils.com).

*moshepa@post.tau.ac.il

¹W. M. Xu, O. Naaman, G. Kh. Rozenberg, M. P. Pasternak, and R. D. Taylor, *Phys. Rev. B* **64**, 094411 (2001); W. M. Xu, M. P. Pasternak, G. Kh. Rozenberg, and R. D. Taylor, *Hyperfine Interact.* **141**, 243 (2002); G. Kh. Rozenberg, M. P. Pasternak, W. M. Xu, L. S. Dubrovinsky, S. Carlson, and R. D. Taylor, *Europhys. Lett.* **71**, 228 (2005).

²A. G. Gavriliuk, V. V. Struzhkin, I. S. Lyubutin, S. G. Ovschinnikov, M. Y. Hu, and P. Chow *Phys. Rev. B* **77**, 155112 (2008), and references therein.

³M. P. Pasternak, G. Kh. Rozenberg, G. Yu. Machavariani, O. Naaman, R. D. Taylor, and R. Jeanloz, *Phys. Rev. Lett.* **82**, 4663 (1999).

⁴J. Staun Olsen, C. S. G. Cousins, L. Gerward, H. Jhans, and B. Sheldon, *Phys. Scr.* **43**, 327 (1991).

⁵G. Kh. Rozenberg, L. S. Dubrovinskii, M. P. Pasternak, O. Naaman, T. Le Bihan, and R. Ahuja, *Phys. Rev. B* **65**, 064112 (2002).

⁶T. Arima, D. Higashiyama, Y. Kaneko, J. P. He, T. Goto, S. Miyasaka, T. Kimura, K. Oikawa, T. Kamiyama, R. Kumai, and R. Tokura, *Phys. Rev. B* **70**, 064426 (2004), and references therein.

- ⁷K. Uk Kang, S. B. Kim, S. Y. An, S. W. Cheong, and C. S. Kim, *J. Mag. Mag. Mat.* **304**, e769 (2006).
- ⁸E. Sterer, M. P. Pasternak, and R. D. Taylor, *Rev. Sci. Instrum.* **61**, 1117 (1990).
- ⁹G. Yu. Machavariani, M. P. Pasternak, G. R. Hearne, and G. Kh. Rozenberg, *Rev. Sci. Instrum.* **69**, 1423 (1998).
- ¹⁰Mössbauer measurements at ambient pressure (Fig. 2) show large line widths compared to the typical line width associated with the natural line width of the 14.4 keV transition in Fe⁵⁷. Previous authors [W. Kim, J. H. We, S. J. Kim, and C. S. Kim, *J. App. Phys.* **101**, M515 (2007)] calculated this Mössbauer spectrum using four Fe sites. In this research, however, the resolution level is not high enough in order to follow the evolution of all four subspectra (and up to six near the phase transition) as a function of pressure, and so their decomposition was forfeited. Considering the limited resolution and the numerical error resulting from it their fit does not differ from ours, and our value of H_{hf} should be taken as an average.
- ¹¹A. P. Hammersley, ESRF Internal Report, ESRF97HA02T (1997).
- ¹²A. P. Hammersley, S. O. Svensson, M. Hanfland, A. N. Fitch, and D. Häusermann, *High Press. Res.* **14**, 235 (1996).
- ¹³A. C. Larson and R. B. Von Dreele, General Structure Analysis System (GSAS), Los Alamos National Laboratory Report LAUR 86-748 (1994).
- ¹⁴B. H. Toby, *EXPGUI, J. Appl. Cryst.* **34**, 210 (2001).
- ¹⁵H. K. Mao, J. Xu, and P. M. Bell, *J. Geophys. Res.* **91**, 4673 (1986).
- ¹⁶A. D. Chijioko, W. J. Nellis, A. Soldatov, and I. F. Silvera, *J. Appl. Phys.* **98**, 114905 (2005).
- ¹⁷Pressure at cryogenic temperature with our DACs, increases slightly, by ~ 1 GPa with respect to RT. This is within the experimental error
- ¹⁸J. C. Jamieson, J. N. Fritz, and M. H. Manghnani, in *High-Pressure Research in Geophysics*, edited by S. Akimoto and M. H. Manghnani (Center for Academic Publishing, Tokyo, 1982), pp. 27–48.
- ¹⁹Y. Kaneko, T. Arima, J. P. He, R. Kumai, and Y. Tokura, *J. Magn. Mater.* **272**, 555 (2004)
- ²⁰O. L. Anderson, *Equations of State of Solids for Geophysics and Ceramic Science* (Oxford University Press, 1994), p. 167.
- ²¹M. Marezio, J. P. Remeika, and P. D. Dernier, *Acta Cryst. B* **26**, 2008 (1970). The extrapolated atomic positions are: Ga: (0.972, 0.082, 0.25), Fe: (0, 0.5, 0), O1: (0.163, 0.416, 0.25), O2: (0.674, 0.321, 0.092).
- ²²The raison d'être for choosing $\Delta V/V_0$ instead of P as the variable are the changes in the bulk modulus taking place while crossing the various several phases along the 0–80 GPa path. The $\Delta V/V_0(P)$ variable does away with this problem.
- ²³N. N. Greenwood and T. C. Gibb, *Mössbauer Spectroscopy* (Chapman and Hall, London, 1971), pp. 46–50.
- ²⁴At a fixed pressure the resistivity data fairly accurately obey the relation of $\ln R = \ln R_0 + E/k_B T$, where k_B is the Boltzmann constant and E the electrical transport activation energy. At the 40–53 GPa range the value of E decreases more than double from 0.37 to 0.17 eV.
- ²⁵The lowest accessible temperature by our cryogenic system.
- ²⁶The relative abundance of the spectral component i is $A_i f_i / \sum_{j=1}^n A_j f_j$ where A_i is the derived value of the area of the absorption component, f_i is the component's recoil-free fraction, and n is the number of components. Here we assume as first approximation, identical values of f for each component
- ²⁷K. Leinenweber, Y. Wang, T. Yagi, and H. Yusa, *Am. Miner.* **79**, 197 (1994); concluded that the HP Pv phases that transform to lithium niobates at LP all have tolerance factors (t) below ~ 0.84 , whereas stable Pv phases have tolerance factors above 0.84. In our case $t = 0.73$, therefore the transition to LN phase at the decompression is expected. (See H. Yusa, M. Akaogi, N. Sata, H. Kojitani, R. Yamamoto, and Y. Ohishi, *Phys. Chem. Minerals* **33**, 217 (2006) and references therein.
- ²⁸H. Boysen and F. Altorfer, *Acta Cryst. B* **50**, 405 (1994). The refined atomic positions are: Ga: (0, 0, 0.307), Fe: (0, 0, 0.0165), O: (−0.01, 0.322, 0.081).
- ²⁹R. Ramirez, L. M. Falicov, and J. C. Kimball, *Phys. Rev. B* **2**, 3383 (1970).
- ³⁰Differences may also arise from the higher sensitivity of the synchrotron XRD method, where the higher signal/noise ratio allows the detection of new components at a level where its relative abundance is too small for Mössbauer spectroscopy.
- ³¹M. Merlini, M. Hanfland, M. Gemmi, S. Huotari, L. Simonelli, and P. Strobel, *Am. Miner.* **95**, 200 (2010).
- ³²H. D. Megaw, *Acta Cryst. A* **24**, 583 (1968).
- ³³X. Wu, G. Steinle-Neumann, O. Narygina, C. McCammon, and L. Dubrovinsky, *High Pressure Research* **30**, 395 (2010).
- ³⁴Y. Sato and S. Akimoto, *J. Appl. Phys.* **50**, 5285 (1979).
- ³⁵L. W. Finger and R. M. Hazen, *J. Appl. Phys.* **51**, 5362 (1980).
- ³⁶The crystallographic transition of the corundum phase into the Rh₂O₃-II structure by itself is accompanied by a volume decrease of $\sim 4\%$ (see R. D. Shannon and C. T. Prewitt, *J. Solid State Chem.* **2**, 134 (1970); N. Funamori and R. Jeanloz, **278**, 1109 (1997). Therefore the part of the volume reduction associated with the electronic transition in Fe₂O₃ is $\sim 6\%$.
- ³⁷R. D. Shannon, *Acta Cryst. A* **32**, 751 (1976).